Nonmonotonic enhancement of diversity-induced resonance in systems of mobile oscillators

Cong Liu, Zhi-Xi Wu,* and Jian-Yue Guan

Lanzhou Center for Theoretical Physics, Key Laboratory of Theoretical Physics of Gansu Province, and Key Laboratory of Quantum Theory and Applications of MoE, Lanzhou University, Lanzhou, Gansu 730000, China and Institute of Computational Physics and Complex Systems, Lanzhou University, Lanzhou, Gansu 730000, China

(Received 23 May 2023; accepted 15 October 2023; published 8 November 2023)

Diversity is omnipresent in natural and synthetic extended systems, the phenomenon of diversity-induced resonance (DIR), wherein a moderate degree of the diversity can provoke an optimal collective response, provides researchers a brand-new strategy to amplify and utilize the weak signal. As yet the relevant advances focus mostly on the ideal situations where the interactions among elements are uncorrelated with the physical proximity of agents. Such a consideration overlooks interactions mediated by the motion of agents in space. Here, we investigate the signal response of an ensemble of spatial mobile heterogeneous bistable oscillators with two canonical interacting modes: dynamic and preset. The oscillators are considered as mass points and perform random walks in a two-dimensional square plane. Under the dynamic scheme, the oscillators can only interact with other oscillators within a fixed vision radius. For the preset circumstance, the interaction among oscillators occurs only when all of them are in a predefined region at the same moment. We find that the DIR can be obtained in both situations. Additionally, the strength of resonance nonmonotonically rises with respect to the increase of moving speed, and the optimal resonance is acquired by an intermediate magnitude of speed. Finally, we propose reduced equations to guarantee the occurrence of such mobility-optimized DIR on the basis of the fast switching approximation theory and also examine the robustness of such phenomenon through the excitable FitzHugh-Nagumo model and a different spatial motion mechanism. Our results reveal for the first time that the DIR can be optimized by the spatial mobility and thus has promising potential application in the communication of mobile agents.

DOI: 10.1103/PhysRevE.108.054209

I. INTRODUCTION

A counterintuitive phenomenon that the system consisting of heterogeneous elements may perform a better role than that of homogeneous ones in inducing an uniform behavior has been verified in disciplines ranging from taming spatiotemporal chaos in nonlinear pendula [1,2], optical wave amplification in physics [3], epidemic contagion and circadian rhythms in biophysics [4–6], complicated spiking activities and advanced cognition in the brain [7–10] to the norm forming in social systems [11]. As striking examples, groups composed of diverse individuals can make more efficient group decisions than that of homogeneous ones in social networks [11]. To achieve stable synchronized networks, selecting the ensemble of heterogeneous oscillators outperforms choosing the homogeneous counterparts, which is known as the converse symmetry breaking [12,13]. The heterogeneous coupling strength is crucial for circadian rhythms [6], to name only a few. Such active role played by diversity or disorder in generating coherent dynamics continue to fascinate researchers especially in fields of statistical physics and complex systems.

Particularly, in 2006, Tessone and coworkers demonstrated that compared to the weak collective response in homogeneous systems, an intermediate degree of disorder can significantly enhance the collective response in physical and neural systems [14]. This phenomenon is called diversity-induced resonance (DIR) [15–17] and has served as a testbed to amplify the weak signal response [16–19], especially. Since then, great efforts have been devoted to extending such resonance-like behavior to more diverse and realistic circumstances. To the best of our knowledge, these advances are mainly concentrated on two directions, the first one is about the sources of diversity, which includes the exogenous and endogenous noise [18], either spatial correlated or uncorrelated quenched disorder [20,21], heterogeneous topological structure (quenched spatial disorder) [22,23] or coupling strength [24–29], time delay in the information transmission [30,31], uniformly distributed periodic signals in forms of Fourier series [32] and even the disordered amplitude [33] or phase delay of the input signal [34,35]. To name one, Liang *et al.* revealed that the disordered initial phases can induce double resonance in globally coupled neurons [34]. The second one focuses on the application scenarios or models, which ranges from Brownian motors [36], electronic circuit [37], linear pendulum [17], chaotic elements [38], threshold devices [39], excitable neuron or medium [40–45], active rotators [46], sleep-wake cycle system [47], coupled hepatocytes [48] to soft matter [49] and social norms [15,50]. For example, Chen and coworkers clarified that the resonance caused by the structural diversity is beneficial to the oscillations of intracellular Ca^{2+} in coupled hepatocytes [48]. Beyond these studies, some state-of-the-art researches play complementary roles in this resonant behavior. For instance, Liang *et al.* verified that the DIR can be obtained even for the circumstance where the

*Corresponding author: wuzhx@lzu.edu.cn

signals are suprathreshold [51]. Liu *et al.* gave the clue that the DIR may be extended to diverse situations, in which the diversity parameters are either symmetrically or asymmetrically distributed [52]. So far, the study of extending and utilizing this resonance-like behavior is an active and expanding field of research [43–45].

All these advances mentioned above have a simple assumption that the interactions among elements are presumed to be persistent for all the course of time, in other words, the interactions between any pair of elements are uncorrelated with the motion of agents in spatial space or physical proximity. However, in a plethora of realistic scenarios, the physical proximity at certain points of time not only dominates the interaction but also influences significantly the collective behavior [53–66]. For example, if the density of desert locusts is above the critical value, then marching locusts will spontaneously and suddenly adopt directed collective motion [67]. In vertebrate somitogenesis, compared to the static cell, dynamic cell movement can not only promote the recovery of synchronization after external perturbation but also support a wider range of reaction parameters [68]. Both the theoretical results and the field observations show that the anti-synchronized choruses and the position in the actual paddy field of the male Japanese tree frogs influence each other [69]. Besides these intriguing biophysical instances, the time-varying interactions in the form of mobile oscillators also influence significantly the transmission of disease [61], the communications of robots [54], the coordination of the traffic [70] and the synchronization or chimera state of networked oscillators [71]. The logical next questions are to ask how the time-varying interactions induced by the spatial mobile elements influence the collective response and whether the phenomenon of DIR can be extended to the mobile oscillators system. The answers to these two questions are much relevant to realistic applications, i.e., the signal propagation in the mobile communication device and the forming of common interests in opinion dynamics. Noteworthy, although a few studies have given the clue that mobility may enhances the signal or epidemic propagation under the scheme of meta-population framework [72,73], how spatial mobility influence the resonance-like phenomenon in the heterogeneous system is rarely reported.

To address these questions, we investigate in this article the collective signal response of an ensemble of spatial moved heterogeneous bistable oscillators, in which the interacting patterns among elements are extracted from the two canonical and realistic scenarios in the collective motion of natural and artificial systems. We find that the DIR can be obtained in both the two interacting schemes. Furthermore, the strength of DIR behaves a bell-shaped curve with respect to the rising of moving speeds, and the optimal DIR can be obtained at an intermediate degree of spatial mobility. We further explore the optimal DIR versus moving speed in the heterogeneous FitzHugh-Nagumo model and under a different mechanism of spatial motion to examine the robustness of such phenomenon.

II. MODEL AND SIMULATION SETTINGS

The numerical results are executed on a two-dimension square-shaped plane with linear size L and periodical boundary. For simplicity, we overlook the influence of the elements shapes and consider the agents as the mass points moving randomly in space. The collective dynamics of the bistable system are composed of the spatial motion of agents and the signal response (state dynamics) of oscillators. The movement of the ith oscillators in space is dominated by

$$\begin{aligned} x_i(t+\Delta t) &= x_i(t) + v\cos(\theta_i(t))\Delta t \mod L, \\ y_i(t+\Delta t) &= y_i(t) + v\sin(\theta_i(t))\Delta t \mod L, \\ \theta_i(t+\Delta t) &= \theta_i(t) + \sqrt{2D_1\Delta t}\xi_i(t) \mod 2\pi, \end{aligned} \tag{1}$$

in which $x_i(t)$, $y_i(t)$, and $\theta_i(t)$ are the position coordinates in the plane and the direction of motion of the ith agent at time t, respectively. In this case, if the absolute speed v equals to zero, then the agents are randomly distributed and unmoved in the two-dimension space. Otherwise, the agents behave random-walk-like diffusion in space with uncorrelated standard Gaussian noise $\xi_i(t)$. The mean value and correlation are $\langle\xi_i(t)\rangle = 0$ and $\langle\xi_i(t)\xi_j(t')\rangle = \delta_{i,j}\delta(t-t')$, respectively, and the constant D_1 dominates the strength of the noise. The initial angle of the ith agent's motion is stochastically chosen from $[0, 2\pi]$ and the Δt represents the motion integration step size.

In present work, the signal response is based on the heterogeneous bistable model, which is a paradigmatic model for signal propagation in physical and biological systems [14,29]. The time evolution of the state of oscillator i is represented by

$$\dot{s}_i = s_i - s_i^3 + \frac{c}{n_i}\sum_{j\in n_i} b_{ij}(s_j - s_i) + a_i + A\sin(\omega t), \quad i = 1, \ldots, N, \tag{2}$$

where $s_i(t)$ is the state variable at moment t, and a_i represents the natural heterogeneity of oscillator i. In general, the diversity parameter a_i is drawn from a Gaussian distribution with mean $\langle a_i\rangle = a_0 = 0$ and variance $\langle(a_i - a_0)(a_j - a_0)\rangle = \delta_{ij}\sigma^2$, where the standard deviation σ measures the degree of diversity among the oscillators. Here, we apply Euclidean distance d_{ij} as the only criteria for judging whether the interaction between pair of oscillators occurs. The symbol b_{ij} is the adjacent matrix at time t, $b_{ij} = 1$ means the interaction occurring between oscillators i and j, and $b_{ij} = 0$ indicates the coupling disappearing. As Fig. 1(a) shows, for the dynamic interacting scheme (also called scheme I hereafter), agents can only interact with others within a fixed range r_c, i.e., $d_{ij} = \sqrt{(x_j - x_i)^2 + (y_j - y_i)^2} < r_c$, called vision radius. This interacting scheme is extracted from the natural collective motion, i.e., the migration of birds and the avoidance of schools of fish, etc. [54,55]. Additionally, the preset interacting scheme (also called scheme II) constrains the interaction emerging only when the agents enter the preset area. For instance, a circular region with the position $(x_0, y_0) = (10, 10)$ as the center and r_c as the radius, see Fig. 1(b), when $d_{io} = \sqrt{(x_i - x_0)^2 + (y_i - y_0)^2} < r_c$ and $d_{jo} = \sqrt{(x_j - x_0)^2 + (y_j - y_0)^2} < r_c$, $b_{ij} = 1$ otherwise $b_{ij} = 0$, which represents the crowds crossed a preset area like intersections and bridges [56,60,62]. The variable n_i measures the total neighbors of oscillators i at the moment t, and c stands for the uniform coupling. The sinusoidal function $A\sin(\omega t)$

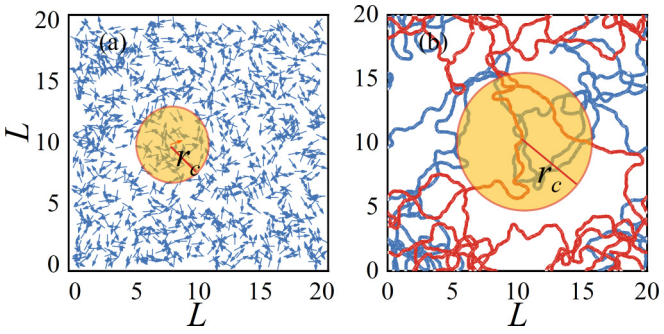

FIG. 1. Graphical illustration of the two canonical interacting schemes. (a) Dynamic interacting region: at every moment, elements can only interact with others within a fixed visual radius r_c. As the oscillators behave random walks in the two-dimension space, the interacting region is moving all the time. (b) Preset interacting region: interactions among elements emerge only when these oscillators enter into a preset circular area with radius r_c.

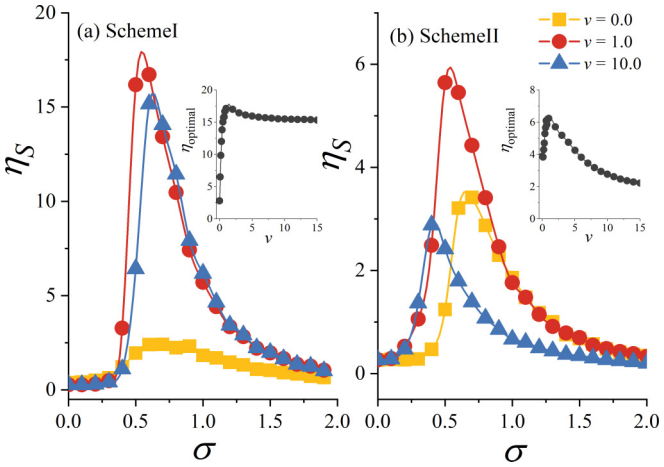

FIG. 2. The spectral amplification factor η_S of Eq. (2) versus the diversity parameters σ under the two interacting schemes for different speeds. The vision radiuses are (a) $r_c = 1.0$ and (b) $r_c = 8.0$, respectively. The optimal collective responses η_{optimal} with respect to diverse absolute speeds of the agents motion are shown in insets. For each absolute speed, we perform σ increases from 0 to 2.0 for one circle and average them for 100 independent circles to calculate the optimal response.

represents the weak stimulus adding into the ith oscillators with amplitude A and frequency ω, respectively. Some parameters are considered as $N = 1000$, $c = 1.0$, $A = 0.2$, $\omega = 2\pi/50$, which are same as the configuration considered in Ref. [14]. The intensity of the noise is fixed to $D_1 = 0.05$. Noteworthy, the collective dynamics are integrated with two distinct time steps: one is for the spatial motion Δt of Eq. (1) and the other is for the state variation $\Delta\tau$ of Eq. (2). Here we consider the two time scales are equal, i.e., $\Delta t = \Delta\tau$ in Ref. [55]. Conventionally, if the variations of the spatial locations of the agents are much slower than their states, i.e., $\Delta t \ll \Delta\tau$, then the interactions among oscillators can be modeled by a static network. On the contrary, if the topology induced by the motions of agents changes fast enough, such as $\Delta t \gg \Delta\tau$, then the effect of the spatial motions of agents is averaged out since one oscillator can interact randomly with any other oscillators. Such a consideration is to avoid these two situations.

The collective response with respect to the weak stimulation can be measured by the spectral amplification η_S [14,29], which is defined as

$$\eta_S = \frac{4}{A^2}|\langle e^{i\omega t} S(t)\rangle|^2, \tag{3}$$

where the average activity of the system is described by $S(t) = N^{-1}\sum_{j=1}^{N} s_j(t)$ and the symbol $\langle ...\rangle$ is time average. The numerical integration of Eqs. (1) and (2) are performed by the Euler method with the integration step size $\Delta t = \Delta\tau = 0.01$ and in each run, the first $50 * T/\Delta t$ steps are deserted and the rest of $50 * T/\Delta t$ steps are utilized to avoid the transient effect. The initial states of oscillator i are chosen randomly from $[-1, 1]$ and the spectral amplification η_S is averaged over 100 independent realizations for each diversity parameter σ.

III. RESULTS AND ANALYSIS

As Fig. 2(a) shows, for the circumstance of static agents, i.e., $v = 0.0$, which can be seen as the nonlocal coupling, as the diversity parameter σ rises, a bell-shaped signal amplification curve where the optimal signal response is $\eta_{\text{optimal}} = 2.5$ can be viewed. This result verifies that the DIR can be extended to the nonlocally coupled system. For an intermediate degree of the absolute speed of the agents motion, such as $v = 1.0$, a significantly enlarged signal response curve can be seen and the optimal signal response rises to 17.7. It demonstrates that the time-varying interaction induced by the spatial motion of the agents has a positive role in improving the DIR phenomenon. For a high level of the speed, say $v = 10.0$, compared to the static situation (the intermediate speed situation), a relatively stronger (weaker) signal amplification curve can be obtained. It suggests that one can acquire an optimal DIR for an intermediate degree of spatial moving speed. A comprehensive description for the influence of the absolute speed on the DIR behavior can be seen in the inset. As the absolute speed increases, the optimal signal response rises rapidly and then declines slowly, which behaves a nonmonotonic enhancement of DIR. These results further confirm that the DIR phenomenon can be promoted by an intermediate degree of motion speeds of the agents. Similar results and conclusions can be observed in the preset situation in Fig. 2(b). Noteworthy, this mobility-optimized DIR phenomenon is robust to the vision radius, noise intensity, particle density, the period of external signal, and even the state-dependent amplitude in which the relationship between the amplitude of external stimulus and the state of oscillator can be either linear or nonlinear functions [76]; see Appendix A.

To address why these distinct magnitudes of resonance phenomenon emerge for different motion speeds, we further consider the individual spectral amplification as

$$\eta_i = \frac{4}{A^2}|\langle e^{i\omega t} s_i(t)\rangle|^2, \tag{4}$$

to investigate the individual signal response of the oscillator i versus the spatial motion of agents.

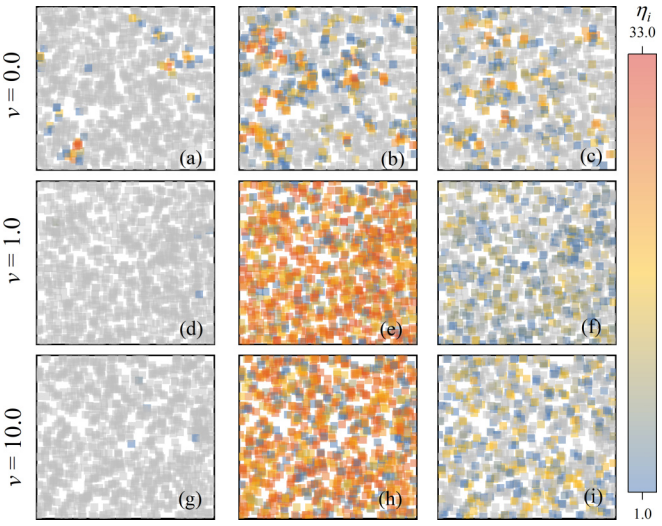

FIG. 3. Spatial distribution of the individual signal response η_i for different absolute speeds under the dynamic scheme. The diversity parameter are (a), (d), (g) $\sigma = 0.2$, (b), (e), (h) $\sigma = 0.6$, and (c), (f), (i) $\sigma = 1.5$, respectively. The gray squares denote the oscillators whose signal response is below 1.0. These maps are the snapshots of spatial distribution of η_i at $t = 100T$.

A. Dynamic interacting region

For the circumstance of static oscillators, like $v = 0.0$, if the diversity is small, say $\sigma = 0.2$, as Fig. 3(a) shows, then only a few elements (6.4 percent of the population size), lie in the top right and bottom left of the cell, respectively, behave enlarged oscillations estimated by whether $\eta_i > 1.0$ [25,29]. For an intermediate degree of diversity, i,e., $\sigma = 0.6$, the number of the enlarged oscillators increases to 39.3 percent of N, these oscillators mainly locate in the top left, top right and bottom left of the square, respectively, see in Fig. 3(b). For a large diversity, $\sigma = 1.5$, not only the number of enlarged oscillators reduces to 27.7 percent of the total oscillators size, but also the amplitude of the individual signal response is reduced; see Fig. 3(c). Although there are a few largely oscillating elements for different σ, i.e., $\eta_{805} = 28.8$ for $\sigma = 0.2$, $\eta_{209} = 30.7$ for $\sigma = 0.6$, and $\eta_{853} = 26.2$ for $\sigma = 1.5$, as the total number of the enlarged oscillators are small, the phenomenon of DIR is thus weak. Nevertheless, for an intermediate speed, i.e., $v = 1.0$, if the diversity is a small value, as Fig. 3(d) shows, then only four oscillators are slightly enlarged. If the diversity is an intermediate value, then a huge number of oscillators, about 99.4 percent of the size of the total oscillators, are amplified and these oscillators distribute uniformly in the cell, see in Fig. 3(e). Reduced amplitude of the individual oscillation as well as the number of amplified oscillators can be seen for large diversity, $\sigma = 1.5$, see in Fig. 3(f). Additionally, similar results can be founded in the situation of large absolute speed, i.e., $v = 10.0$, where the amplitude of the individual oscillation is slightly weaker than that of the corresponding situation for $v = 1.0$, as shown in Figs. 3(g)–3(i). These results further disclose that compared to the locally coupled situation, the time-varying coupling in the form of mobile oscillators can significantly enhance the DIR.

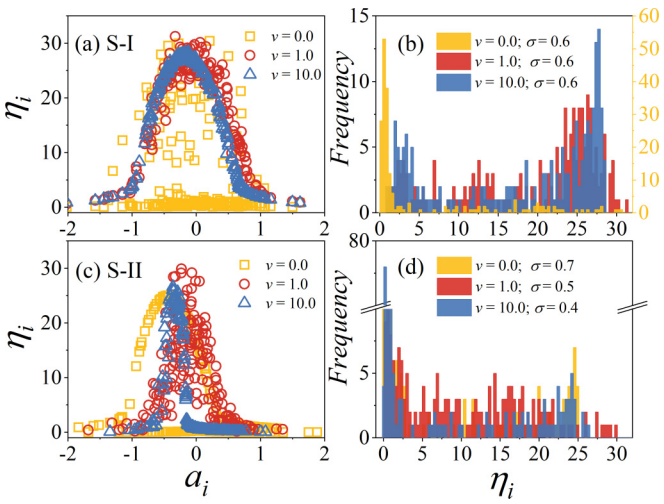

FIG. 4. The individual signal response η_i distributions with respect to the diversity parameter a_i for different absolute speeds under the (a) dynamic and (c) preset schemes, respectively. For the dynamic scheme, the diversity for the optimal signal response is equal to 0.6 for the three speeds, and the corresponding frequency distributions of the individual signal responses are shown in panel (b). Whereas for the preset scheme, the optimal diversity configurations are 0.7, 0.5, and 0.4 for $v = 0.0$, $v = 1.0$, and $v = 10.0$, respectively. The corresponding frequency distribution of the individual signal response are shown in panel (d). For clarity, 200 oscillators that chosen randomly from the oscillators pool are in our consideration. Similar results can be found for the sampling of all oscillators.

For comparison, we also give the individual signal response distribution with respect to the diversity parameter and the corresponding frequency distributions at the optimal diversity for different moving speeds. As Fig. 4(a) shows, for $v = 0.0$, the individual signal responses mainly concentrate in low extent region and a few individual responses dispersedly distribute in the strong response area. For $v = 10.0$, the individual responses behave a bell-shaped strip region and compactly spread over the area of $\eta = 0.0 \sim \eta = 28.7$. For $v = 1.0$, similar bell-shaped yet more dispersed distribution with a higher individual response compared to the situation of $v = 10.0$ can be seen. Specifically, see Fig. 4(b), for static oscillators, although a few of the oscillators behave enlarged response, the remaining oscillators are weak-enlarged, thus the ensemble response represents a weak resonance. For a large moving speed, the frequency distribution showcases two peaks, the low one lying in a weak-amplified region and the other high one locates near $\eta = 27$. However, for an intermediate speed, while the frequency distribution resembles that of the large moving speed, the scene that a relative higher ratio of the strong-amplified oscillators can be seen. As a consequence, the optimal DIR can be obtained at an intermediate moving speed.

Now we recall the microscopic mechanism of the diversity-induced resonance. If there are none of oscillators in the vision radius, i.e., $n_i = 0$, then the potential of Eq. (2) is read as $V(s_i) = -0.5s_i^2 + 0.25s_i^4 - a_i s_i - As_i \sin(\omega t)$. Without the addition of diversity and external stimulus, say $a_i = 0$ and $A = 0$, all oscillators will get absorbed in one of the two steady states, $s_1^* = 1$ or $s_2^* = -1$, which correspond to the two

minima of $V(s)$. For the situation of a homogeneous system with a weak stimulus, i.e., $a_i = 0$ and $A < A_{\rm th} = \sqrt{4/27}$, the potential of Eq. (2) tilts periodically with the external force but the barrier that forbids the interwells oscillation remains. Consequently, the oscillators jiggle slightly near one of the bottoms of $V(s)$, and no resonance-like behavior will be observed. Particularly, for a heterogeneous system, the potential is no longer symmetrical due to the natural diversity, i.e., if the diversity parameter of an oscillator is $a_1 = 0.5$, then the left potential is deeper than the right one during the first half period. Because the tilt induced respectively by diversity and external signal is superimposed, the oscillator can overcome the barrier occasionally. But for the subsequent half period, the inclines evoked by the diversity and external signal are conflicted and canceled, the oscillators cannot go back to the original potential well if there are absence of coupling inputs. Nevertheless, thanks to the coupling pull of the oscillators (whose diversity parameters are negative, i.e., $a_2 = -0.5$), both the positive and negative oscillators can overcome the barrier and the obvious resonance can be detected [29]. For the circumstance of $v = 0$, as the oscillators randomly distribute in the 2D space, the oscillators can only interact with a few oscillators, $\pi r_c^2 N/L^2 \approx 7$, consequently, the successful resonance match of the oscillators is infrequent, the collective signal response is thus weak. For spatial mobile oscillators, during the detecting periods, the number of the oscillators that inject the coupling input to the target oscillator is significantly promoted, such resonance match rises and consequently the DIR can be improved by the spatial motion of the particles.

We now describe the mechanism mentioned above analytically. The dynamics of Eqs. (1) and (2) can be translated into the form $\dot{s}_i = F(s_i) - c\sum_{j=1}^{N} g_{ij}(t)s_j$, in which $F(s)$ represents the individual dynamic of every single oscillator, $g_{ij}(t)$ are the elements of a time-varying matrix $G(t)$ which defines the neighborhood of each oscillator at a given moment t, $g_{ij}(t) = g_{ji}(t) = -1$ if the oscillators ith and jth are neighbors at time t. On the basis of the fast switching theory, where the entries of the time-varying connectivity matrix can be replaced by the probability that two agents are within the coupling range, as if the time-varying topology changes fast enough. Namely, the time averaged matrix $\overline{G} = \frac{1}{T}\int_t^{t+T} G(\tau)d\tau$ can be replaced by $\overline{G} = p_A G_A + p_0 G_0$, in which G_A and G_0 represent the static connectivity matrices within and without nonzero elements, respectively [55,65]. For the sake of simplicity, here we consider two oscillators situation. At each moment t, only four network configurations are observed: (i) None of interaction between the two oscillators exist. (ii) An unidirectional coupling from node 2 to node 1 can be observed. (iii) An unidirectional interaction from node 1 to node 2 exists. (iv) A bidirectional interaction between the two nodes is shown. If we consider the symbols p_{00}, p_{12}, p_{21}, and $p_{\rm global}$ as the link probabilities for the four situations and $G_{00} = \left[\begin{smallmatrix}0 & 0\\ 0 & 0\end{smallmatrix}\right]$, $G_{12} = \left[\begin{smallmatrix}1 & -1\\ 0 & 0\end{smallmatrix}\right]$, $G_{21} = \left[\begin{smallmatrix}0 & 0\\ -1 & 1\end{smallmatrix}\right]$, and $G_{\rm global} = \left[\begin{smallmatrix}1 & -1\\ -1 & 1\end{smallmatrix}\right]$ are the corresponding Laplacian matrices, then the time averaged matrix read as $\overline{G} = p_{00}G_{00} + p_{12}G_{12} + p_{21}G_{21} + p_{\rm global}G_{\rm global}$. Since $p_{12} = p_{21}$, $\overline{G} = p_A G_{\rm global} = p_A G_A$, in which $p_A = p_{12} + p_{\rm global}$ can be viewed as the probability that the two nodes are neighbors.

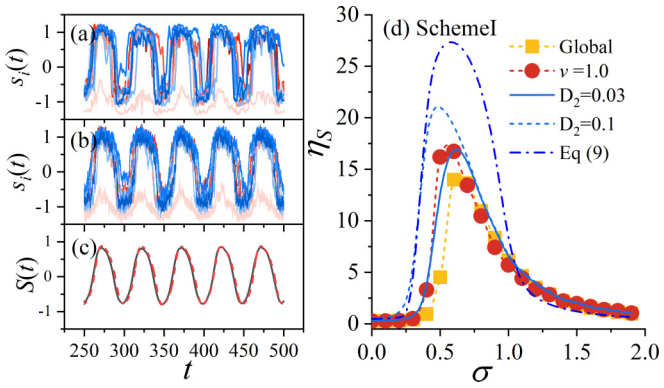

FIG. 5. (a) The timeseries of ten oscillators chosen randomly from the oscillators pool of Eq. (2) for $v = 1.0$ and $\sigma = 0.6$. (b) The corresponding ten timeseries under the noisy coupling scheme of Eq. (5) for $D_2 = 0.03$ and $\sigma = 0.6$. The serial numbers of oscillators are the same as in panel (a). (c) The average dynamics of Eqs. (2) and (5) for $\sigma = 0.6$. (d) The spectral amplification factor η_S versus diversity parameter σ for distinct situations.

As the initial positions of the two agents are randomly distributed in the 2D space, under the static conditions, say $v = 0$, the probability that agent 2 is within the version radius r_c is given by $p_A = \pi r_c^2/L^2$. These results can be extended to the large size system in which the oscillator size $N \gg 2$, but the diagonal and nondiagonal elements of the corresponding matrix G_A are $N-1$ and -1, respectively. Taking into account the density of the particles, one can obtain $p_A = \pi r_c^2 \rho/N$ and $\overline{G} = \pi r_c^2 \rho G_A/N$. These results demonstrate that as the moving speed rises to a large value, the time-varying network approaches to a rescaled all-to-all network. As a consequence, the DIR can be significantly enhanced via mobile oscillators.

On the one hand, depending on such analysis, we can find that as the moving speed rises, the coupling scheme undergoes the transition process from local to nonlocal and subsequently to global. However, for a purely static network, the optimal DIR emerges in the all-to-all network configuration since as the coupling range (distance) rises to $N/2$, the optimal DIR monotonically increases to the maximum; see Appendix B. On the other hand, for the spatial static oscillators, the coupling inputs for every oscillator are determinate, but for the mobile oscillators, such coupling inputs are noisy, see Fig. 5(a), and the intensity of fluctuation decreases as the moving speed rises [55]. One can further confirm the noisy coupling from two aspects: first, at each moment, the coupling function of Eq. (2) can be seen as a local mean-field $c(S_{\rm cluster} - s_i)$, $S_{\rm cluster} = \frac{1}{n_i}\sum_{j=1}^{n_i} s_j$, where the oscillators within the vision radius are random on the basis of the Eq. (1), the coupling input thus is noisy. Second, as the diversity is a source of static disorder, which could not induce the fluctuating dynamics, the noisy timeseries shown in Fig. 5(a) are purely evoked by the fluctuating coupling input. We thus speculate that the noisy coupling input, especially for intermediate value of moving speeds, plays a positive role in inducing the nonmonotonic behavior.

To verify such speculate, we consider a globally coupled bistable system with every element has an additional independent noisy coupling injection. For the mobile oscillators

system, at every moment which oscillator interacts with the target oscillator is not determined, but the coupling injection on the target oscillator is noisy all the time. Consequently, we consider a noisy injection accompanied with the target oscillator to represent the randomness of coupling, namely, the subscript of independent noise equals the one of the target oscillator. Such equation describes the scene where the moving speed is an intermediate value, i.e., the coupling range is large the coupling injections however are still noisy although the intensity is weak, which can be represented by

$$\dot{s}_i = s_i - s_i^3 + \frac{c}{N}\sum_{j=1}^{N}(s_j - s_i + \zeta_i(t)) + a_i + A\sin(\omega t),$$
$$i = 1, \ldots, N, \tag{5}$$

in which ζ_i is uncorrelated Gaussian white noise with zero mean and autocorrelation $\langle \zeta_i(t)\zeta_j(t')\rangle = 2D_2\delta_{i,j}\delta(t - t')$, where D_2 is the noise intensity. As Fig. 5(d) shows, compared to the nonnoisy situation which corresponds to the globally coupled system, a weak noisy coupling can significantly enlarge the DIR. Furthermore, the resonance phenomenon in mobile oscillators, $v = 1.0$, can be reasonably reproduced by the noisy coupling model Eq. (5), say $D_2 = 0.03$, both in the ensemble signal response, average oscillation and the specific dynamics of the corresponding oscillators, see Figs. 5(a)–5(c).

For further analysis, Eq. (5) can be reduced to

$$\dot{s}_i = s_i - s_i^3 + c(S - s_i + \zeta_i(t)) + a_i + A\sin(\omega t). \tag{6}$$

Summing first the N terms of Eq. (6) and then averaging them, one can obtain the collective dynamics

$$\dot{S} = S - S^3 - 3S^2\langle\delta_i\rangle_N - 3S\langle\delta_i^2\rangle_N - \langle\delta_i^3\rangle_N,$$
$$+\sqrt{\frac{2c^2D_2}{N}}\xi(t) + A\sin(\omega t), \tag{7}$$

in which $\delta_i(t) = s_i(t) - S(t)$ denotes the deviation of ith oscillator from the collective dynamics, the sign $\xi(t)$ is the Gaussian white noise having the same properties as $\zeta_i(t)$, and the symbol $\langle\ldots\rangle_N$ is the oscillators average. A conventional approach in reducing the Eq. (7) in statistical mechanics is Gaussian approximation [74,75], in which δ_i can be treated as independent Gaussian variables with zero mean and variance $M = \langle\delta_i^2\rangle_N$. Consequently, the odd moments, i.e., $\langle\delta_i\rangle_N$, $\langle\delta_i^3\rangle_N$ can be neglected and Eq. (7) can be reduced to

$$\dot{S} = (1 - 3M)S - S^3 + \sqrt{\frac{2c^2D_2}{N}}\xi(t) + A\sin(\omega t). \tag{8}$$

Furthermore, taking the correlation $W = \delta_i a_i$ into consideration, one can obtain the closed ordinary differential equation with truncation in third order

$$\dot{S} = (1 - 3M)S - S^3 + \sqrt{\frac{2c^2D_2}{N}}\xi(t) + A\sin(\omega t),$$
$$\dot{M} = 2M(1 - 3S^2 - c - 3M) + 2D_2 + 2W,$$
$$\dot{W} = W(1 - 3S^2 - c - 3M) + \sigma^2. \tag{9}$$

The major differences between Eq. (9) and the reduced equations in Ref. [74] are the items of diversity and the coupling-dependent noise. For a homogeneous system, Eq. (9) is equal to the reduced equations in Ref. [74] for $c = 1.0$. For a heterogeneous system, significant differences between the two schemes can be found, as shown in Appendix C. For instance, without coupling one can still obtain an enlarged signal response because stochastic resonance can emerge in the isolated oscillators for the reduced equations in Ref. [74]. Nevertheless, only a weak and constant signal response can be viewed in Eq. (9) since noise vanishes and DIR cannot occur in isolated oscillators. Inserting Eq. (9) into Eq. (3), one can get a semianalytic signal response curve. As Fig. 5(d) shows, the bell-shaped curve of Eq. (9) reasonably captures the resonance behavior in Eq. (5), and further demonstrate that a weak noisy coupling adding in the mean-field form can enhance the DIR. As a consequence, for an intermediate degree of moving speed, analytically, there is a higher resonant response than that of the high speed situation. Further analyses of Eq. (9) for strong coupling situations are shown in Appendix D.

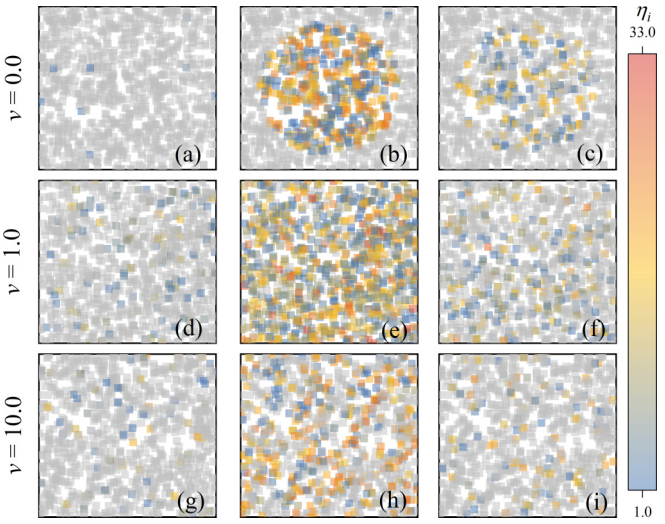

FIG. 6. Spatial distribution of the individual signal response η_i for different absolute speeds under the preset scheme. The diversity parameters are (a), (d), (g) $\sigma = 0.2$, (b) $\sigma = 0.7$, (e) $\sigma = 0.5$, (h) $\sigma = 0.4$, and (c), (f), (i) $\sigma = 1.5$, respectively. The gray squares denote the oscillators whose signal response is below 1.0. These maps are the snapshots of spatial distribution of η_i at $t = 100T$.

B. Preset interacting region

For the scheme of preset interacting region, if the moving speed is absent, as Figs. 6(a)–6(c) show, then a weak heterogeneity can only evoke a few oscillators, about 0.8% of the system size, to oscillate in the form of slight enhancement. But an intermediate degree of diversity can induce a large number of elements, nearly 46%, to oscillate sharply. Since the coupling are restricted in the circle region, all enlarged oscillators distributed in this coupling region. As the strong heterogeneity can weaken the resonance, compared to the situation of $\sigma = 0.7$, the scene that weak individual response oscillators distributed in the coupling region can be found, in which not only the individual signal responses are weaker but also the number of the enlarged oscillators is decreased. Nevertheless, for an intermediate level moving speed, i.e.,

$v = 1.0$, the oscillators of which the signal responses are enlarged are no longer restricted in the circle coupling region, see Figs. 6(d)–6(f), these oscillators homogeneously scatter in the 2D plane. The reason for such status is that when the resonant oscillators leave from the coupling region to the coupling blind area, the coupling inputs vanish immediately, and their oscillations, however, still continue. Since the individual signal response η_i is a longstanding average quantity, it will not decrease to a small value instantly (a similar delayed result can be found when the oscillators leave from the coupling blind area to the coupling region). Consequently, the distinct signal responses can be viewed in the whole space rather than only in the coupling region in the snapshots. Especially, for $\sigma = 0.5$, a mass of oscillators, about 83% of the total number of the system, are enlarged, which reveals a stronger DIR can be viewed compared to the static oscillators. Additionally, for a high moving speed, compared to the circumstance of $v = 1.0$, an obvious reduction of the enlarged oscillators can be seen for all the range of diversity parameters.

We also give the individual signal response distribution and frequency distribution under the optimal diversity for distinct moving speeds to compare the resonance explicitly. As Fig. 4(c) shows, for $v = 0.0$, the individual signal response split into two different strip areas in the $a_i - \eta_i$ space: a bell-shaped strip and a horizontal band, which corresponds to the resonant behavior in coupling region and the weak oscillations in coupling blind areas, respectively. For $v = 1.0$, canopy-like individual signal response distribution with higher peak and more crowded heap can be viewed. For $v = 10.0$, not only the peak of the distribution decreases, but also the density of the enlarged signal response reduces. Additionally, as Fig. 4(d) shows, for the situations of $v = 0.0$ and $v = 10.0$, the vast majority of the oscillators have slightly oscillations with $\eta_i < 2.0$, and only a small fraction of the oscillators behave drastically oscillations with $18.0 < \eta_i < 25.0$. However, for an intermediate degree of moving speed, the fraction of weak individual signal response significantly decreases, and not only the ratio of strong signal response rises obviously, but also the maximum signal response rises to 33. These results further support that spatial motion can significantly enhance the DIR for the preset coupling scheme, and an intermediate level of moving speed can evoke the optimal resonant behavior.

The mechanism behind the mobility-optimized DIR is that compared to weak resonance in restricted coupling region, due to the spatial motion, the oscillators that originally lie in the coupling blind areas can enter into the coupling region and be enlarged. As a consequence, an enhanced resonance can be found. Nevertheless, when the moving speed is large, during every half of the oscillation period, the agents across the coupling region over and over again, each stay in the coupling region is brief, the coupling is flickering. The interwell oscillations need time windows, the fast-disappearing coupling thus weakens the resonance.

IV. ROBUSTNESS DETECTION

To examine the robustness of the nonmonotonic enhancement of DIR in mobile oscillators, we first consider the other

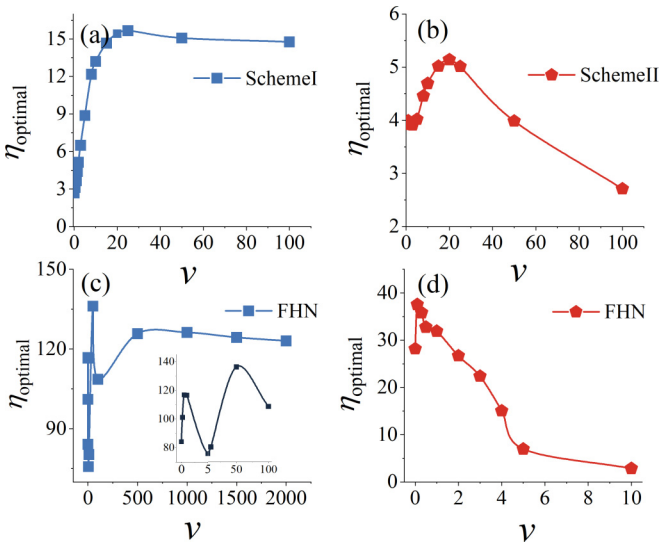

FIG. 7. The optimal collective response $\eta_{optimal}$ with respect to the absolute speeds of agents motion for different spatial motion and state evolution. The dynamics of agents motion in 2D space for (a) dynamic and (b) preset schemes are dominated by Eq. (10), nevertheless the state evolution still follows Eq. (2). The state dynamics of oscillators for (c) dynamic and (d) preset schemes are followed by Eq. (11), whereas the spatial motions are based on Eq. (1). The inset in panel (c) is the zoom-in of the same figure for $v = 0$ to $v = 100$.

conventional model of mobile oscillators, in which the directions of ith agent φ_i at each moment are randomly selected with uniform probability in the interval $[-\pi, \pi]$ [55,61,65]. The spatial motion can be described as

$$\begin{aligned} x_i(t + \Delta t) &= x_i(t) + v\cos(\theta_i(t))\Delta t \mod L, \\ y_i(t + \Delta t) &= y_i(t) + v\sin(\theta_i(t))\Delta t \mod L, \\ \theta_i(t + \Delta t) &= \varphi_i(t + \Delta t), \end{aligned} \tag{10}$$

and the state dynamics of the oscillators are same as Eq. (2). As Figs. 7(a) and 7(b) show, although the region of moving speed extends to a relative high level, the nonmonotonic resonance enhancement can still be viewed for both the two coupling schemes.

Second, we translate the bistable oscillators into more complicated and biologically relevant excitable elements: the archetypical FitzHugh-Nagumo model [7,14,43,44], of which the dynamics can be represented by

$$\begin{aligned} \epsilon\dot{s}_i &= s_i - \frac{1}{3}s_i^3 - u_i + \frac{c}{n_i}\sum_{j\in n_i} b_{ij}(s_j - s_i), \\ \dot{u}_i &= s_i + a_i + A\sin(\omega t), i = 1, \ldots, N, \end{aligned} \tag{11}$$

where s_i and u_i are the fast membrane potential and the slow potassium gating variable of the ith element, respectively. The spatial motions of excitable elements are still follow the Eq. (1). The parameter $\epsilon = 0.01$ characterizes the timescale separation between the fast and slow variables. The diversity parameters are randomly chosen from the Gaussian distribution of mean $\langle a_i \rangle = a_0$ and correlations $\langle (a_i - a_0)(a_j - a_0) \rangle = \delta_{ij}\sigma^2$. Here, we consider the parameters configuration as Ref. [14] chose: $a_0 = 1.12$, $c = 1.0$,

$A = 0.05$, and $T = 5.0$. In Fig. 7(c), a multi-peaks-like optimal signal response enhancement can be viewed through increasing the speed of the spatial motion under the dynamic coupling scheme as a relative strong noise which corresponds to the situation of a small moving speed can also weaken the DIR. Furthermore, under the preset coupling scheme, the optimal signal response increases first and then decreases, which represents a single-peak resonance enhancement; see Fig. 7(d). All these results demonstrate that compared to the static situation, the spatial motion of agent can evoke the nonmonotonic enhancement of diversity-induced resonance.

V. CONCLUSIONS

In conclusion, we have systematically investigated the celebrated phenomenon: diversity-induced resonance in mobile oscillators through two realistic and conventional spatial motion schemes: the dynamic coupling area in the form of vision radius and the static preset coupling region. We found that compared to the resonance in static oscillators, the spatial motion can significantly enhance the resonance magnitude. Besides, an optimal diversity-induced resonance can be obtained by an intermediate degree of moving speed. Furthermore, such nonmonotonic enhancement of diversity-induced resonance is robust to the different spatial random motion mechanisms of agents and the dynamical models of states.

Noteworthy, although the DIR has been extended to diverse situations and been investigated in more profound ways, at least one important issue remains hard to address: whether natural systems have taken advantage or not from this diversity-induced collective effect. To our knowledge, one origin of the difficulty is the unrealistic coupling assumption. Although the DIR can be viewed as a particular case of stochastic resonance (SR) [14], SR can be obtained in the single-particle system, while the interaction among distinct particles is necessary for the emergence of DIR. Up to this day, most numerical experiments and theoretical predictions on DIR are based on the static coupling assumption where the coupling function is uncorrelated with the spatial motion of agents. Since one signature of realistic systems is that the interactions among elements are dominated by the physical proximity of agents. Our results, although they are still about the numerical experiments and theoretical predictions, reveal for the first time that the time-varying coupling in the form of mobile oscillators may plays a significant role in DIR, and consequently may provide a new clue to answer the question that whether natural systems can utilize the diversity-induced resonance.

ACKNOWLEDGMENTS

C.L. thanks professors Xiaoming Liang (in Jiangsu Normal University) and Xiyun Zhang (in Jinan University) for helpful discussions. We acknowledge financial support from the National Natural Science Foundation of China (Grants No. 11975111 and No. 12247101), and from the Fundamental Research Funds for the Central Universities (Grant No. lzujbky-2023-ey02). We thank the anonymous reviewers for critical comments that helped improve the paper.

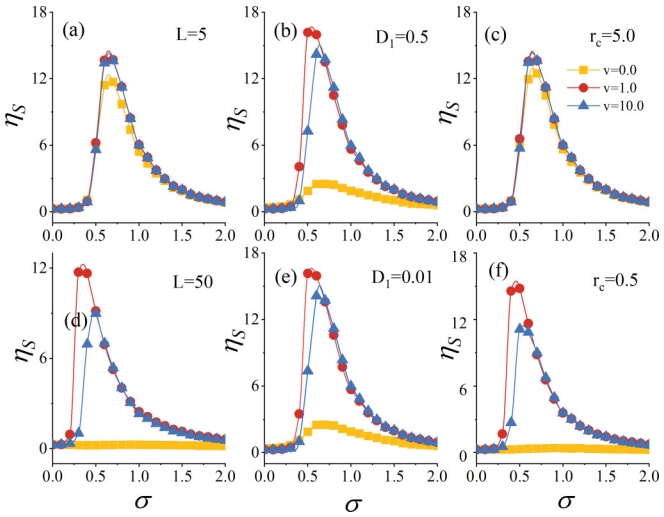

FIG. 8. The phenomenon of mobility-optimized DIR for (a) high and (d) low particle densities, the oscillators size is fixed to 1000, thus one can obtain a high (low) particle density for a short (long) boundary, (b) strong and (e) weak noise strengths, (c) big and (f) small vision radiuses under the dynamic scheme.

APPENDIX A: ROBUSTNESS EXAMINATION FOR DIFFERENT VISION RADIUS, NOISE INTENSITY, PARTICLE DENSITY, AMPLITUDES OR PERIODS OF THE EXTERNAL SIGNALS

As Fig. 8 shows, under the dynamic coupling scheme, for the situation of a relative high particle density, the moving speed strengthens the DIR, although the optimal resonance magnitudes at intermediate and high speed level are approximative, one can still find that the optimal DIR occurs at the intermediate moving speeds; see Fig. 8(a). For a low particle density, if the moving speed is zero, then the phenomenon of

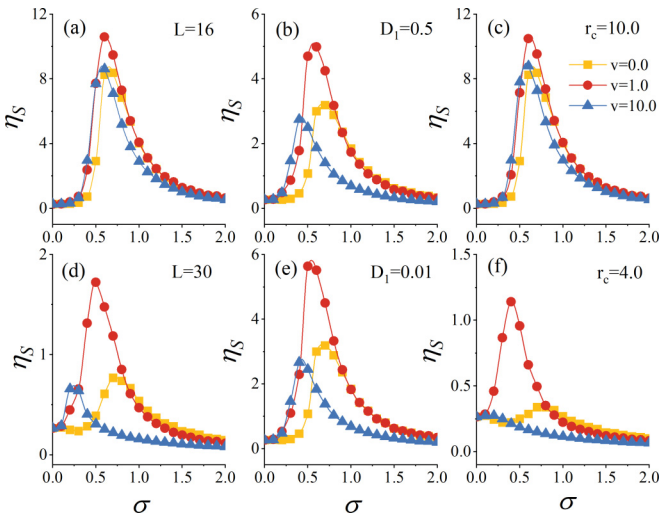

FIG. 9. The phenomenon of mobility-optimized DIR for (a) high and (d) low particle densities, the oscillators size is fixed to 1000, thus one can obtain a high (low) particle density for a short (long) boundary, (b) strong and (e) weak noise strengths, (c) big and (f) small vision radiuses under the preset scheme.

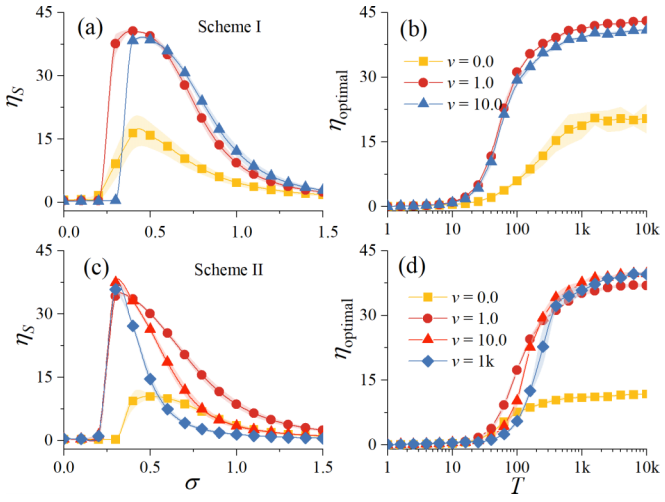

FIG. 10. The collective signal response η_S with respect to diversity under (a) the dynamic coupling scheme and (c) the preset coupling scheme for different moving speeds. The optimal signal response versus the period of the external driving force for different moving speeds under (b) the dynamic coupling scheme and (d) the preset coupling scheme.

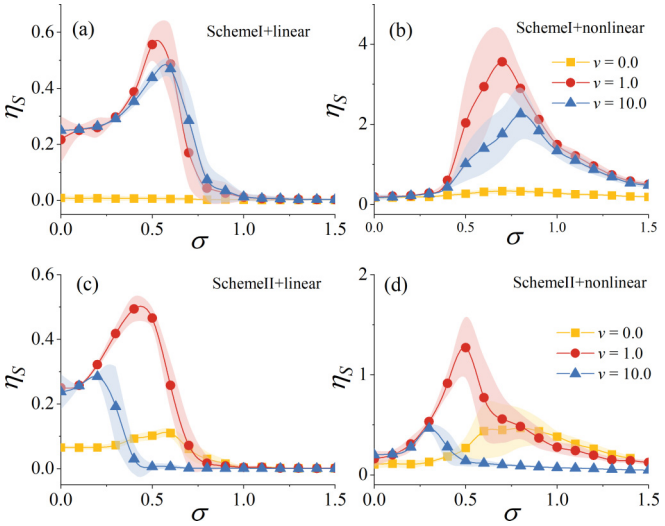

FIG. 11. The collective signal response η_S with respect to diversity for different moving speeds with the state-dependent amplitude of the external driving force. The dynamic coupling scheme with (a) linear function $f(s_i) = s_i$, (b) nonlinear function $f(s_i) = 0.5[1 + \tanh(s_i)]$. The preset coupling scheme with same (c) linear and (d) nonlinear functions. The period of the external driving force is $T = 50$.

DIR nearly disappears, and consequently the strengthening influence of spatial motion on DIR is remarkable; see Fig. 8(d). These results of high and low particle densities resemble those of big and small vision radius, respectively; see Figs. 8(c) and 8(f). Furthermore, we can find that the influence of the noise intensity of the motion's direction on the mobility-optimized DIR is weak; see Figs. 8(b) and 8(e). These results demonstrate that such mobility-optimized DIR is robust for diverse vision radius, noise intensity, and particle density under the dynamic scheme (also under preset scheme, see Fig. 9). We further explore the influence of the period of the external signal on the behavior of mobility-optimized DIR. Following the avenue of Ref. [14], we first consider the DIR within different moving speeds for a large period signal, i.e., $T = 1000$, under both the dynamic and preset schemes. As Fig. 10(a) shows, compared to the signal response in the static situation, the mobility of agents can significantly enhance the resonance. Furthermore, the optimal DIR can be found under the situation of the intermediate degree of moving speeds. Similar results can be found for the preset scheme as well, see Fig. 10(c). It is worth noting that although the strength of DIR for speed $v = 10.0$ is no longer weaker than that of $v = 1.0$, for a sufficient large speed, the magnitude of DIR is weaker again than that of $v = 10.0$; consequently, the phenomenon of the nonmonotonic enhancement of DIR is still robust.

Second, since resonance-like behavior is strongly related to the frequency of the driving signal [76], i.e., when the frequency of the external driving force approaches to the natural oscillation frequency the maximum amplitude of oscillation can be viewed. We thus explore the magnitude of the DIR (in form of η_{optimal}) versus the period of the external driving force for different moving speeds. For the dynamic scheme, see Fig. 10(b), the magnitude of DIR rises in a S-shape as the increase of the period, which is coincide with the corresponding results in Fig. 1 of Ref. [14]. Furthermore, one can find that the optimal DIR curve corresponds to the situation of the intermediate moving speed, i.e., $v = 1.0$. Additionally, similar results for the preset scheme can be found in Fig. 10(d). These results demonstrate that the phenomenon of mobility-optimized DIR is robust for the period (frequency) of the external driving force. Noteworthy, for the small period signals, since the oscillator cannot jump from one well to the other during the small time window that the potential barrier disappears and recovers, thus the amplitude of the oscillation remains small for all ranges of diversity. Additionally, since the amplitude of the external signal is not always fixed and homogeneous, we further investigate the influence of the heterogeneous external driving forces in the form of the state-dependent amplitude on the phenomenon of mobility-optimized DIR. The state evolution of bistable oscillators thus can be represented by

$$\dot{s}_i = s_i - s_i^3 + \frac{c}{n_i}\sum_{j\in n_i} b_{ij}(s_j - s_i) + a_i + Af(s_i)\sin(\omega t),$$
$$i = 1, \ldots, N. \tag{A1}$$

The spatial motion is still a random-walk-like diffusion as considered in the main text. To reveal the universality (arbitrariness) of the selected function $f(\cdot)$, we consider two typical functional forms: the linear function, i.e., $f(s_i) = s_i$, and the nonlinear function, say, $f(s_i) = 0.5[1 + \tanh(gs_i)]$ [76].

As Fig. 11 shows, although the resonance is weak compared to the situation where the amplitudes of the external driving forces are homogeneous, one can still observe that the optimal DIR emerges in an intermediate moving speed for both the linear and nonlinear functions. These results further demonstrate that the phenomenon of the mobility-optimized DIR is robust.

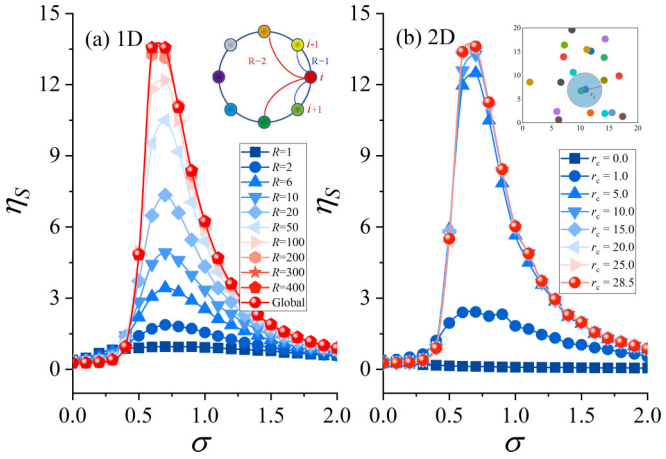

FIG. 12. The dependence of the DIR on the coupling range in (a) one-dimension ring and (b) two-dimension square, respectively.

APPENDIX B: DIR VERSUS THE COUPLING RANGE IN 1D AND 2D SPACE

To clarify the dependence of DIR on the coupling range, we first consider a one-dimension ring, the dynamics of which can be read as

$$\dot{s}_i = s_i - s_i^3 + \frac{c}{2R}\sum_{j=i-R}^{j=i+R}(s_j - s_i) + a_i + A\sin(\omega t),$$
$$i = 1, \ldots, N, \tag{B1}$$

in which R represents the coupling range; see the inset of Fig. 12(a). The parameters configuration is the same as that chosen in the main text. As Fig. 12(a) shows, with the increasing of coupling range, the strength of DIR rises, and the optimal DIR corresponds to the global coupling situation. Moreover, for the two-dimension square, we continue to use the dynamic coupling scheme but without spatial motion of agent. As the inset of Fig. 12(b) shows, if the vision radius r_c is vanishing, then all the oscillators are isolated. As r_c increases, the coupling range rises as well. If $r_c > 20\sqrt{2}$, then no matter where the agent lies in the space, it can interact with all other agents, which can be viewed as the global coupling situation. As Fig. 12(b) shows, the optimal DIR sill occurs in the global coupling situation. These results further sustain the conclusion in the main text that for a purely static network, the optimal DIR emerges in the all-to-all network configuration since as the coupling range (distance) rises to $N/2$, the optimal DIR monotonically increase to maximum.

APPENDIX C: THE DIFFERENCES AND SIMILARITIES BETWEEN EQ. (9) AND THE DESAI-ZWANZIG MODEL

In this Appendix, we give the similarities and differences between the reduced equations (i.e., the model used by Pikovsky and coworkers in Ref. [74], since such a model is a standard model used in statistical physics and commonly referred to as Desai-Zwanzig model, for convenience, we call them Desai-Zwanzig model) and the order parameter equation [Eqs. (7), (8), or (9) in the main text]. The order parameter

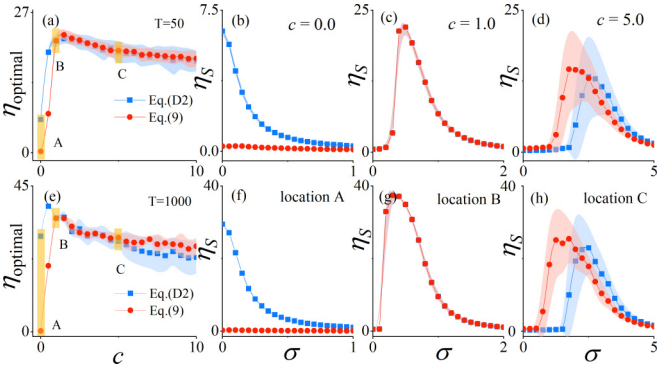

FIG. 13. The differences and similarities between the Desai-Zwanzig model and the order parameter equation for different periods of the external signals. (a) The optimal signal response versus coupling for small-period signal ($T = 50$). Three couplings (b) $c = 0.0$, (c) $c = 1.0$, and (d) $c = 5.0$ are considered in detail to reveal the differences and similarities. The same objectives under the situation of large-period signal ($T = 1000$) are shown in panels (e)–(h).

equation can be reduced to the Desai-Zwanzig model if the diversity is vanished. Besides, the major differences of these two models are whether the white noise terms are coupling-dependent for a heterogeneous system, consequently, we pay more attention to explore the optimal signal response versus the coupling strength. As Fig. 13(a) shows, when $c = 1.0$, the optimal signal responses for the two models are equal. However, if $c < 1.0$, then the optimal signal response of the Desai-Zwanzig model is significantly larger than that of the order parameter equation in the main text. Especially, for a vanishing coupling, one can still observe the enlarged signal response, i.e., $\eta_{\text{optimal}} = 6.4$, because of the stochastic resonance effect. Whereas the optimal signal response of the order parameter equation is weak, say $\eta_{\text{optimal}} = 0.26$, since the noise term disappears and DIR cannot emerge in the isolated oscillators system. Furthermore, when $c > 1.0$, the optimal signal response of the order parameter equation is slightly larger than that of the Desai-Zwanzig model. To investigate the signal response η_S versus the diversity detailedly, there couplings, i.e., $c = 0.0$, $c = 1.0$, and $c = 5.0$ are in our consideration. As Fig. 13(b) shows, for $c = 0.0$, despite no DIR emerges under both the two models, the signal response of the Desai-Zwanzig model is larger than that of the order parameter equation, especially for a small diversity. For $c = 1.0$, as Fig. 13(c) shows, the two signal responses are equal for all the diversity parameters. Furthermore, when $c = 5.0$, on the one hand, the magnitude of the DIR for the order parameter equation is slightly larger than that of the Desai-Zwanzig model. On the other hand, the optimal diversity parameter which corresponds to the optimal signal response is smaller than that of the Desai-Zwanzig model; see Fig. 13(d). Similar results can be obtained for the situation of large period signal; see Figs. 13(e)–13(h). These results demonstrate that the order parameter equation can be reduced to the reduced equation used by Pikovsky and coworkers in Ref. [74] for a homogeneous system for $c = 1.0$. For a heterogeneous system, the signal response has significant differences between these two models.

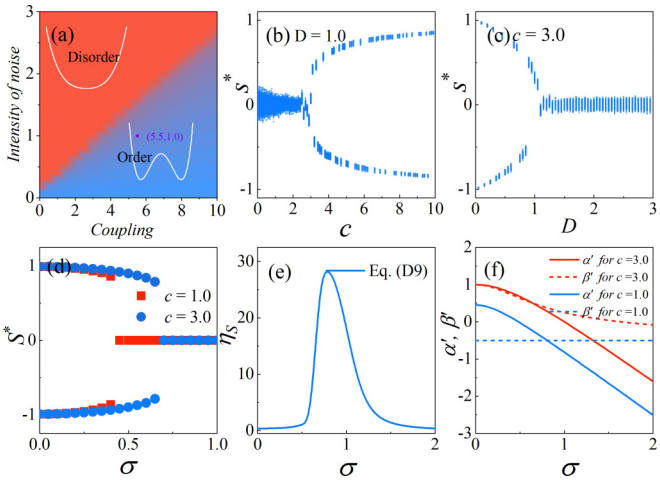

FIG. 14. (a) The phase transition process of Eq. (D1). The red and blue regions denote $s^* = 0$ and $s^* = 1$, respectively. (b) The order parameter versus coupling for fixed noisy intensity. (c) The order parameter with respect to noise intensity for fixed coupling. (d) The dependence of the order parameter $S^* = \langle S \rangle_t$ of Eq. (D7) on diversity. (e) The signal response of Eq. (D9) for $c = 3.0$. (f) The coefficients of the linear and cubic terms of Eq. (D9) versus the diversity.

APPENDIX D: FURTHER ANALYSIS FOR THE COLLECTIVE SIGNAL RESPONSE

In this Appendix, we give the reduction analysis and linear response (used by Pikvosky and coworkers in Ref. [74]) for the collective signal response of Eq. (9) [Eq. (9) in the main text], and we discuss the feasibility through which to obtain the analytical expression of the signal response η_S.

We first recall the analysis processes used in Ref. [74]. The globally coupled bistable oscillators with noise and weak external driving force is read as

$$\dot{s}_i = s_i - s_i^3 + \frac{c}{N}\sum_{j=1}^{N}(s_j - s_i) + \sqrt{2D}\xi_i + A\sin(\omega t),$$
$$i = 1, \ldots, N. \tag{D1}$$

If we consider $s^* = \langle S \rangle_t$ in which $S = \frac{1}{N}\Sigma s_i$ as the order parameter, as Fig. 14(a) shows, then we can find an Ising-type phase transition because of the competition between noise-induced disorder and coupling-evoked order. More detailed, for a fixed noise intensity, i.e., $D = 1.0$, if the coupling is less than the critical value, then the order parameter fluctuates around the $s^* = 0$ as the noise-induced disorder outperform the coupling-caused order, whereas when the coupling overcomes the critical coupling, since the order forming of the elements, the order parameter approaches to $s^* = \pm 1$; see Fig. 14(b). For a fixed coupling, the opposite effect can be viewed as the noise increases; see Fig. 14(c).

For the disorder phase, the potential function of the order parameter has only one stable fixed point $s^* = 0$, while for the order phase, three fixed points with one unstable $s^* = 0$ and two stable $s^* = \pm 1$ exist. If one selects the parameter configuration in the order phase, i.e., $c = 5.5$ and $D = 1.0$ (the configuration considered in Ref. [74]), then since the effective noise decreases as the system size rises, the situation of three fixed points thus always exists. For instance, the order parameter evolution

$$\dot{S} = (1 - 3M)S - S^3 + \sqrt{\frac{2D}{N}}\xi(t) + A\sin(\omega t),$$
$$\dot{M} = 2M(1 - 3S^2 - c - 3M) + 2D, \tag{D2}$$

in which $\delta_i = s_i - S$ and $M = \frac{1}{N}\sum \delta_i^2$, has three fixed points with two stable $S^{*2} = [2 - c + \sqrt{(2+c)^2 - 24D}]/4$ and one unstable $S_0^* = 0$, in which $M_{12}^* = [2 + c - \sqrt{(2+c)^2 - 24D}]/12$ and $M_0^* = [1 - c + \sqrt{(1-c)^2 - 12D}]/6$. Near the bifurcation point, utilizing the slaving principle, i.e., $\dot{M} = 0$, one can obtain the one-dimensional equation in form of the standard noise-driven bistable system

$$\dot{S} = aS - bS^3 + \sqrt{\frac{2D}{N}}\xi(t) + A\sin(\omega t), \tag{D3}$$

where $a = 0.5(c+1) - 0.5\sqrt{(c-1)^2 + 12D}$ and $b = -0.5 + 1.5(c-1)/\sqrt{(c-1)^2 + 12D}$. Taking advantage of the linear response formula obtained in stochastic resonance with the normal form of double-well potential, one can obtain the analytical collective response

$$R = \frac{NS^{*2}}{2Da}\left(\frac{\mathcal{D}_{-3/2}(-\sqrt{X})}{\mathcal{D}_{-1/2}(-\sqrt{X})}\right)^2\left[1 + \frac{\pi^2\omega^2}{2a^2}\exp(X)\right]^{-1}, \tag{D4}$$

where $X = aNS^{*2}/2D$, and $\mathcal{D}$ are the parabolic cylinder functions. Since

$$\mathcal{D}_{-n-\frac{1}{2}}\left(-\frac{1}{\sqrt{2D}}\right) \approx \frac{\sqrt{2\pi}}{\Gamma\left(n+\frac{1}{2}\right)}\exp\left(\frac{1}{8D}\right)2D^{\frac{1}{4}-\frac{1}{2}n}, \tag{D5}$$

in which $\Gamma(3/2) = \sqrt{\pi}/2$ and $\Gamma(1/2) = \sqrt{\pi}$. As a consequence,

$$R = \frac{NS^{*2}}{D^2 a}\left[1 + \frac{\pi^2\omega^2}{2a^2}\exp(X)\right]^{-1}. \tag{D6}$$

Now we consider the situation of the noisy coupling assisted DIR, i.e., the collective signal response in form of the three-dimensional order parameter equation in main text,

$$\dot{S} = (1 - 3M)S - S^3 + \sqrt{\frac{2c^2D_2}{N}}\xi(t) + A\sin(\omega t),$$
$$\dot{M} = 2M(1 - 3S^2 - c - 3M) + 2D_2 + 2W,$$
$$\dot{W} = W(1 - 3S^2 - c - 3M) + \sigma^2. \tag{D7}$$

On the basis of the adiabatic elimination, one can assume $\dot{W} = 0$, and thereby obtain $W = \sigma^2/-(1 - 3S^2 - c - 3M)$. For a rough simplification, say $W = \sigma^2$, we can further reduce Eq. (D7) as

$$\dot{S} = (1 - 3M)S - S^3 + \sqrt{\frac{2c^2D_2}{N}}\xi(t) + A\sin(\omega t),$$
$$\dot{M} = 2M(1 - 3S^2 - c - 3M) + 2D_2 + 2\sigma^2. \tag{D8}$$

To obtain the fixed points, we consider $\dot{S} = 0$ and $\dot{M} = 0$ and then have $S_{\text{trivial}}^* = 0$, $S_{\text{untrivial}}^{*2} = 1 - 3M_{\text{untrivial}}^*$, $M_{\text{trivial}}^* = (1 - c + \sqrt{(1-c)^2 + 12(D+\sigma^2)})/6$ and M_{untrival}^*

$= (1 - c - 3S^2 + \sqrt{(1 - c - 3S)^2 + 12(D + \sigma^2)})/6$. Utilizing $S^{*2}_{\text{untrivial}} = 1 - 3M^*_{\text{untrivial}}$, we can obtain $M^*_{\text{untrival}} = (c + 2 - \sqrt{(c + 2)^2 - 24(D + \sigma^2)})/12$ and $S^{*2}_{\text{untrivial}} = (2 - c + \sqrt{(c + 2)^2 - 24(D + \sigma^2)})/4$. Near the bifurcation point, following the slaving principle, we can obtain the one-dimensional equation in form of the standard noise-driven bistable system as well,

$$\dot{S} = a'S - b'S^3 + \sqrt{\frac{2c^2 D_2}{N}}\xi(t) + A\sin(\omega t), \qquad \text{(D9)}$$

in which $a' = 0.5(c + 1) - 0.5\sqrt{(c - 1)^2 + 12(D + \sigma^2)}$ and $b' = -0.5 + 1.5(c - 1)/\sqrt{(c - 1)^2 + 12(D + \sigma^2)}$. The signal response of Eq. (D9) are shown in Fig. 14(e). Noteworthy, as we mentioned earlier, the reduction analysis is on the basis of the order phase, in which the potential function of the order parameter has three fixed points. However, as Fig. 14(d) shows, when diversity parameter rises, the situation where three fixed points coexist translates into the the case in which only one stable fixed point exists. Furthermore, a larger coupling causes a wider scope of diversity for using the reduction methods. Consequently, Eq. (D9) is reasonable at large coupling strength.

Following the linear response, one can obtain the analytical signal response as

$$\eta_S = \frac{NS^{*2}_{\text{untrivial}}}{(D + \sigma^2)^2 a'}\left[1 + \frac{\pi^2\omega^2}{2a'^2}\exp(X')\right]^{-1}, \qquad \text{(D10)}$$

in which $X' = a'NS^{*2}_{\text{untrivial}}/2(D + \sigma^2)$. Nevertheless, the analytical signal response Eq. (D10) is not proper, because of the coefficients of the first and third terms in Eq. (D9) are not the constants, furthermore, these coefficients can be negative values as diversity increases, see Fig. 14(f).

[1] Y. Braiman, J. F. Lindner, and W. L. Ditto, Nature (London) **378**, 465 (1995).
[2] S. F. Brandt, B. K. Dellen, and R. Wessel, Phys. Rev. Lett. **96**, 034104 (2006).
[3] A. M. Perego, Phys. Rev. A **106**, L031505 (2022).
[4] B. F. Nielsen, L. Simonsen, and K. Sneppen, Phys. Rev. Lett. **126**, 118301 (2021).
[5] N. Komin, A. C. Murza, E. Hernández-García, and R. Toral, Interface Focus **1**, 167 (2011).
[6] C. Gu, J. H. T. Rohling, X. Liang, and H. Yang, Phys. Rev. E **93**, 032414 (2016).
[7] C. Zhou, J. Kurths, and B. Hu, Phys. Rev. Lett. **87**, 098101 (2001).
[8] J. F. Mejias and A. Longtin, Phys. Rev. Lett. **108**, 228102 (2012).
[9] S. J. Tripathy, K. Padmanabhan, R. C. Gerkin, and N. N. Urban, Proc. Natl. Acad. Sci. USA **110**, 8248 (2013).
[10] S. Rich, H. M. Chameh, J. Lefebvre, and T. A. Valiante, Cell Rep. **39**, 110863 (2022).
[11] B. Karamched, M. Stickler, W. Ott, B. Lindner, Z. P. Kilpatrick, and K. Josić, Phys. Rev. Lett. **125**, 218302 (2020).
[12] T. Nishikawa and A. E. Motter, Phys. Rev. Lett. **117**, 114101 (2016).
[13] Y. Zhang, J. L. Ocampo-Espindola, I. Z. Kiss, and A. E. Motter, Proc. Natl. Acad. Sci. USA **118**, e2024299118 (2021).
[14] C. J. Tessone, C. R. Mirasso, R. Toral, and J. D. Gunton, Phys. Rev. Lett. **97**, 194101 (2006).
[15] C. J. Tessone, A. Sánchez, and F. Schweitzer, Phys. Rev. E **87**, 022803 (2013).
[16] R. Toral, C. J. Tessone, and J. V. Lopes, Eur. Phys. J. Spec. Top. **143**, 59 (2007)
[17] R. Toral, E. Hernandez-Garcia, and J. D. Gunton, Int. J. Bifurcat. Chaos **19**, 3499 (2009).
[18] C. J. Tessone, A. Scirè, R. Toral, and P. Colet, Phys. Rev. E **75**, 016203 (2007).
[19] T. Pérez, C. R. Mirasso, R. Toral, and J. D. Gunton, Philos. Trans. R. Soc. A **368**, 5619 (2010).
[20] D. Wu, S. Zhu, and X. Luo, Phys. Rev. E **79**, 051104 (2009).
[21] L. Wu, S. Zhu, X. Luo, and D. Wu, Phys. Rev. E **81**, 061118 (2010).
[22] J. A. Acebrón, S. Lozano, and A. Arenas, Phys. Rev. Lett. **99**, 128701 (2007).
[23] H. Chen, Y. Shen, Z. Hou, and H. Xin, Chaos **19**, 033122 (2009).
[24] T. Vaz Martins, R. Toral, and M. A. Santos, Eur. Phys. J. B **67**, 329 (2009).
[25] T. Vaz Martins, V. N. Livina, A. P. Majtey, and R. Toral, Phys. Rev. E **81**, 041103 (2010).
[26] T. Vaz Martins and R. Toral, Prog. Theor. Phys. **126**, 353 (2011).
[27] X. Liang, C. Liu, and X. Zhang, Phys. Rev. E **101**, 022205 (2020).
[28] C. Liu and X. Liang, Phys. Rev. E **100**, 032206 (2019).
[29] C. Liu, Z. X. Wu, C. Y. Wang, H. X. Yang, and J. Y. Guan, Chaos **33**, 013114 (2023).
[30] J. Tang, J. Ma, M. Yi, H. Xia, and X. Yang, Phys. Rev. E **83**, 046207 (2011).
[31] Y. B. Jia, X. L. Yang, and J. Kurths, Chaos **24**, 043140 (2014).
[32] P. J. Martínez and R. Chacón, Phys. Rev. E **93**, 042311 (2016).
[33] M. Gosak, D. Korošak, and M. Marhl, New J. Phys. **13**, 013012 (2011).
[34] X. Liang, M. Dhamala, L. Zhao, and Z. Liu, Phys. Rev. E **82**, 010902(R) (2010).
[35] X. Liang and X. Zhang, Phys. Rev. E **104**, 034204 (2021).
[36] D. Wu and S. Zhu, Phys. Rev. E **85**, 061101 (2012).
[37] C. Yao and M. Zhan, Phys. Lett. A **374**, 2446 (2010).
[38] H. Chen and J. Zhang, Phys. Rev. E **77**, 026207 (2008).
[39] H. Chen, Z. Hou, and H. Xin, Physica A **388**, 2299 (2009).
[40] M. Gassel, E. Glatt, and F. Kaiser, Phys. Rev. E **76**, 016203 (2007).
[41] E. Glatt, M. Gassel, and F. Kaiser, Phys. Rev. E **75**, 026206 (2007).
[42] M. Grace and M. T. Hütt, Eur. Phys. J. B **87**, 29 (2014).
[43] S. Scialla, A. Loppini, M. Patriarca, and E. Heinsalu, Phys. Rev. E **103**, 052211 (2021).
[44] S. Scialla, M. Patriarca, and E. Heinsalu, Europhys. Lett. **137**, 51001 (2022).

[45] M. E. Yamakou, E. Heinsalu, M. Patriarca, and S. Scialla, Phys. Rev. E **106**, L032401 (2022).
[46] X. M. Liang, L. Zhao, and Z. H. Liu, Eur. Phys. J. B **85**, 219 (2012).
[47] M. Patriarca, E. Hernández-Garcíab, and R. Toral, Chaos Solitons Fractals **81**, 567 (2015).
[48] H. Chen, J. Zhang, and J. Liu, Phys. Rev. E **75**, 041910 (2007).
[49] M. Perc, M. Gosaka, and S. Kralj, Soft Matter **4**, 1861 (2008).
[50] C. J. Tessone and R. Toral, Eur. Phys. J. B **71**, 549 (2009).
[51] X. Liang, L. Zhao, and X. Zhang, Chaos **30**, 103101 (2020).
[52] C. Liu, C. Y. Wang, Z. X. Wu, H. X. Yang, and J. Y. Guan, Chaos **32**, 083112 (2022).
[53] P. Holme and J. Saramäki, Phys. Rep. **519**, 97 (2012).
[54] D. Ghosh, M. Frasca, A. Rizzo, S. Majhi, S. Rakshit, K. Alfaro-Bittner, and S. Boccaletti, Phys. Rep. **949**, 1 (2022).
[55] M. Frasca, A. Buscarino, A. Rizzo, L. Fortuna, and S. Boccaletti, Phys. Rev. Lett. **100**, 044102 (2008).
[56] M. Frasca, A. Buscarino, A. Rizzo, and L. Fortuna, Phys. Rev. Lett. **108**, 204102 (2012).
[57] M. Starnini, A. Baronchelli, and R. Pastor-Satorras, Phys. Rev. Lett. **110**, 168701 (2013).
[58] D. Tanaka, Phys. Rev. Lett. **99**, 134103 (2007).
[59] L. Prignano, O. Sagarra, and A. Díaz-Guilera, Phys. Rev. Lett. **110**, 114101 (2013).
[60] S. N. Chowdhury, S. Majhi, M. Ozer, D. Ghosh, and M. Perc, New J. Phys. **21**, 073048 (2019).
[61] M. Frasca, A. Buscarino, A. Rizzo, L. Fortuna, and S. Boccaletti, Phys. Rev. E **74**, 036110 (2006).
[62] B. Kim, Y. Do, and Y.-C. Lai, Phys. Rev. E **88**, 042818 (2013).
[63] X. Ling, W.-B. Ju, N. Guo, C.-Y. Wu, and X.-M. Xu, Phys. Lett. A **384**, 126881 (2020).
[64] H.-X. Yang, W.-X. Wang, Y.-B. Xie, Y.-C. Lai, and B.-H. Wang, Phys. Rev. E **83**, 016102 (2011).
[65] N. Fujiwara, J. Kurths, and A. Díaz-Guilera, Phys. Rev. E **83**, 025101(R) (2011).
[66] F. Peruani, E. M. Nicola, and L. G. Morelli, New J. Phys. **12**, 093029 (2010).
[67] J. Buhl, D. J. T. Sumpter, I. D. Couzin, J. J. Hale, E. Despland, E. R. Miller, and S. J. Simpson, Science **312**, 1402 (2006).
[68] K. Uriu, Y. Morishita, and Y. Iwasaa, Proc. Natl. Acad. Sci. USA **107**, 4979 (2010).
[69] I. Aihara, T. Mizumoto, T. Otsuka, H. Awano, K. Nagira, H. G. Okuno, and K. Aihara, Sci. Rep. **4**, 3891 (2014).
[70] H.-X. Yang, W.-X. Wang, Y.-B. Xie, Y.-C. Lai, and B.-H. Wang, Europhys. Lett. **98**, 68003 (2012).
[71] L. A. Smirnov, M. I. Bolotov, G. V. Osipov, and A. Pikovsky, Phys. Rev. E **104**, 034205 (2021).
[72] C. Shen, H. Chen, and Z. Hou, Europhys. Lett. **102**, 38004 (2013).
[73] C. Shen, H. Chen, and Z. Hou, Chaos **24**, 043125 (2014).
[74] A. Pikovsky, A. Zaikin, and M. A. de la Casa, Phys. Rev. Lett. **88**, 050601 (2002).
[75] R. Desai and R. Zwanzig, J. Stat. Phys. **19**, 1 (1978).
[76] B. Cessac, Chaos **29**, 103105 (2019).